

# Interacting warm dark matter

Norman Cruz,<sup>a</sup> Guillermo Palma,<sup>a</sup> David Zambrano<sup>a</sup> and Arturo Avelino<sup>b</sup>

<sup>a</sup>Departamento de Física, Facultad de Ciencia,  
Universidad de Santiago de Chile,  
Casilla 307, Santiago, Chile.

<sup>b</sup>Departamento de Física, DCI, Campus León,  
Universidad de Guanajuato,  
CP. 37150, León, Guanajuato, México.

E-mail: [norman.cruz@usach.cl](mailto:norman.cruz@usach.cl)

**Abstract.** We explore a cosmological model composed by a dark matter fluid interacting with a dark energy fluid. The interaction term has the non-linear  $\lambda\rho_m^\alpha\rho_e^\beta$  form, where  $\rho_m$  and  $\rho_e$  are the energy densities of the dark matter and dark energy, respectively. The parameters  $\alpha$  and  $\beta$  are in principle not constrained to take any particular values, and were estimated from observations. We perform an analytical study of the evolution equations, finding the fixed points and their stability properties in order to characterize suitable physical regions in the phase space of the dark matter and dark energy densities. The constants  $(\lambda, \alpha, \beta)$  as well as  $w_m$  and  $w_e$  of the EoS of dark matter and dark energy respectively, were estimated using the cosmological observations of the type Ia supernovae and the Hubble expansion rate  $H(z)$  data sets. We find that the best estimated values for the free parameters of the model correspond to a warm dark matter interacting with a phantom dark energy component, with a well goodness-of-fit to data. However, using the Bayesian Information Criterion (BIC) we find that this model is overcome by a warm dark matter – phantom dark energy model without interaction, as well as by the  $\Lambda$ CDM model. We find also a large dispersion on the best estimated values of the  $(\lambda, \alpha, \beta)$  parameters, so even if we are not able to set strong constraints on their values, given the goodness-of-fit to data of the model, we find that a large variety of their values are well compatible with the observational data used.

**Keywords:** Interacting model, phantom dark energy, warm dark matter

---

## Contents

<b>1</b>	<b>Introduction</b>	<b>1</b>
<b>2</b>	<b>General considerations of an interacting dark sector</b>	<b>3</b>
2.1	Effective EoS for interacting fluids	3
2.2	The behavior of the coincidence parameter $r$	4
2.3	Case $w_m = 0$	5
2.4	Case $w_m > 0$ (warm dark matter)	5
<b>3</b>	<b>Evolution equations: Fixed points and stability analysis</b>	<b>5</b>
<b>4</b>	<b>Numerical analysis</b>	<b>8</b>
4.1	Symmetry for $w_e$ and $w_m$	8
4.2	Spiral trajectories	8
<b>5</b>	<b>Observational Constraints</b>	<b>9</b>
5.1	The Hubble parameter	9
5.2	Cosmological probes	11
5.2.1	Type Ia Supernovae	12
5.2.2	Hubble expansion rate	14
<b>6</b>	<b>Discussion and Conclusions</b>	<b>16</b>

---

## 1 Introduction

The existence of a dark component with an exotic equation of state, i. e., with a ratio  $w = p/\rho$  negative and close to  $-1$ , which drives an accelerated expansion, is consistent with data coming from type Ia Supernovae (SNe Ia) [1], large scale structure formation (LSS) [2], cosmic microwave background radiation (CMB) [3], baryon acoustic oscillations (BAO) [4] and weak lensing [5].

Cosmic observations show that densities of dark energy (DE) and dark matter (DM) are of the same order today, despite their different decreasing rates. To solve the so-called coincidence problem [6] an evolving dark energy field with a non-gravitational interaction with matter [7] is proposed (decay of dark energy to dark matter). In this case both dark fluids interact via an additional coupling term in the fluid equations. In the current research different forms of coupling have been considered. Most of them study the coupling between cold DM and DE. In general, the interactions investigated are particular cases the form  $\lambda_m H \rho_m + \lambda_e H \rho_e$ , where  $H$  is the Hubble parameter, and  $\rho_m, \rho_e$  are the dark matter and dark energy densities respectively [8].

Nevertheless, non linear interactions of the form  $\lambda \frac{\rho_m \rho_e}{\rho_m + \rho_e}$  were considered in [9]. A more plausible interaction is inspired by the situation of two types of fluids interacting, where the interaction is proportional to the product of the powers of the energy density of both components. In this case, the interaction rate goes to zero as one or both densities become zero, and increases when each of the densities grows. We then consider in this paper a general interaction of the form  $\lambda \rho_m^\alpha \rho_e^\beta$ , where the parameter  $\lambda$  has dimensions of  $[\text{energy-density}^{\alpha+\beta-1} \times \text{time}]^{-1}$ .

This type of interaction was investigated in the framework of an holographic dark energy [10] and in coupled quintessence [11, 12], where the evolution of the energy densities of the dark interacting components was investigated for different values of the parameters  $\alpha$  and  $\beta$ . A cyclic scenario for the present situation  $\rho_e \sim \rho_m$  was found as a possible solution to the coincidence problem. The particular case  $\alpha = \beta = 1$  was studied in [13]. In this case, if energy is transferred from dark energy to dark matter ( $\lambda > 0$ ), and for phantom type dark energy ( $w_e < -1$ ), the energy densities also display periodic orbits. A general result, which is independent of the interaction type, and only assumes that the energy is transferred from dark energy to dark matter, pointed out that stationary solutions for the ratio  $r = \rho_m/\rho_e$  require a phantom dark energy [14].

Nevertheless, these stationary solutions do not guarantee a solution of the coincidence problem. For example, in [15] a DE modelled by a phantom field was studied in the framework of interaction terms proportional to a density. The results of this investigation indicates that in all cases the late-time solutions correspond to a complete DE domination and as a consequence the coincidence problem remains unsolved. A suitable coupling, with the form  $\frac{\rho_e \rho_m}{\rho_e + \rho_m}$ , was chosen in [16] for a phantom field evolving under an exponential potential. An accelerated late-time phase with a stationary ratio of the energies densities of the two components was found.

The requirement of phantom DE to obtain stationary solutions can be seen as a kind of theoretical need for this type of matter in the framework of an interacting dark sector. From the observational point of view, phantom DE is supported by new SN Ia data [17] [18], analysis of the cosmic microwave background (CMB) and large-scale structure. This model is also preferred by WMAP data combined with either SNe Ia or baryon acoustic oscillations (BAO). Nevertheless, from the theoretical point, fluids that violate the null energy condition  $\rho + p \geq 0$  present problems, such as UV quantum instabilities of the vacuum [19]. For a phantom DE with constant EoS parameter  $w_e$ , its the late time behavior is characterized by an increasing energy density which becomes infinite in a finite time (Big Rip). The interaction of a phantom fluid with dark matter can prevent this type of behavior, leading to finite energy densities during the cosmic evolution and avoiding of future singularities.

The aim of this paper is to study the time evolution of the dark sector densities when the interaction mentioned above is considered. This evolution is driven by a highly non-linear coupled differential equations when the parameters  $\alpha$  and  $\beta$  are left free. We solve numerically these equations and also study analytically the stability of the fixed-points. Since it has been argued that the second law of thermodynamics and Le Châtelier's principle implies  $\lambda > 0$  [20] we do not consider here the case of energy transferred from dark matter to dark energy.

In most of the previous investigation which take into account this type of non lineal interaction, cold dark matter with zero pressure is taken to be interacting with the dark energy fluid. Nevertheless, current research has opened the possibility that a warm dark matter component fits better new results found at the level of galaxies and cluster of galaxies [21]. For a wide discussion on this matter see [22].

When both dark fluids are under interaction, their effective EoS behaves following Eq. (2.5) (see below in Section II). For cold dark matter, the effective EoS always corresponds to an exotic fluid with negative pressure, nevertheless for warm dark matter the effective EoS parameter could change the sign during the cosmic evolution. Since up to date we do not know which is the nature of this matter, the proposed model together with observations allow either exotic dark matter or warm dark matter. An interacting warm dark matter allows these two possibilities and so it assumes from the beginning a positive EoS constant

parameter for this component.

In this work we investigate how a warm dark matter modifies the behavior of an interacting dark sector and the constraints for its EoS (assuming a barotropic form) derived from astrophysical observations.

Our paper is organized as follows. In section 2 we present the effective equations of state for the interacting dark components, assuming that the energy is transferred from dark energy to dark matter. We also extend the result found in [14] in order to find the condition for stationary points of the parameter  $r$  when the dark matter is assumed not to be dust. In section 3 we study the two coupled differential equations corresponding to continuity equations of both interacting fluids. We study analytically the fixed-points including their stability. In section 4, we obtain numerical solutions using a numerical method of adaptive step-size algorithm called Bulirsch-Stoer method. We explore the behavior of the fixed points varying the parameters  $\alpha$ ,  $\beta$  and the EoS of both dark sector components. In section 5 we use result from cosmological observation to find the best values for the free parameters,  $(\alpha, \beta, \lambda, w_m)$ , of the corresponding theoretical model. Finally, in section 6 the main results are summarized and different physical scenarios consistent with cosmological observations are discussed.

## 2 General considerations of an interacting dark sector

In the following we assume a flat FRW universe filled basically with the fluids of the dark sector. We consider a warm dark matter of density  $\rho_m$  and a dark energy component described by the density  $\rho_e$ . For simplicity we also assume that both fluids obey a barotropic EoS, so we have  $p_m = w_m \rho_m$  for the warm dark matter and  $p_e = w_e \rho_e$  for the dark energy. In what follows we restrict our model to the late time of cosmic evolution, which implies that the others components of the universe, like radiation and baryons are negligible. In this case the sourced Friedmann equation is given by

$$3H^2 = \rho_m + \rho_e, \quad (2.1)$$

where  $8\pi G = 1$  has been adopted. We will assume that the dark matter component is interacting with the dark energy component, so their continuity equations take the form

$$\dot{\rho}_m + 3(1 + w_m)H\rho_m = +Q \quad (2.2)$$

$$\dot{\rho}_e + 3(1 + w_e)H\rho_e = -Q, \quad (2.3)$$

where  $H = \dot{a}/a$  is the Hubble parameter, and  $a(t)$  is the scale-factor. Here, an overdot indicates a time derivative.  $Q$  represents the interaction term, despite that we do not use a specific functional dependence at this stage, we will only assume that  $Q$  do not change its sign during the cosmic evolution.

### 2.1 Effective EoS for interacting fluids

Let us discuss briefly the behavior of the dark components in terms of an effective EoS driven by the interacting term. Rewriting the continuity equation (2.2) in the usual form

$$\dot{\rho}_m + 3(1 + w_{m_{eff}})H\rho_m = 0, \quad (2.4)$$

where  $w_{m_{eff}}$  represents the effective EoS for the interacting dark matter, which is given by

$$w_{m_{eff}} = w_m - \frac{Q}{3H\rho_m}. \quad (2.5)$$

Note that the behavior of  $w_{m_{eff}}$  can be quite different if  $w_m$  is non zero. With the usual assumption of cold dark matter ( $w_m = 0$ ) and  $Q > 0$ , which implies that energy is transferred from dark energy to dark matter, some kind of exotic dark matter with a negative EoS is driven, assuming, of course, that we are in an expanding universe  $H > 0$ . For warm dark matter we would have, depending on the type of interaction considered and the strength of the coupling constant appearing in  $Q$ , a possible change of the sign on the effective EoS during the cosmic evolution. For the dark energy, the effective EoS is given by

$$w_{\Lambda_{eff}} = w_e + \frac{Q}{3H\rho_e}. \quad (2.6)$$

For  $Q > 0$  the above equation indicates, even for  $w_e = -1$  (cosmological constant), that the effective Dark Energy (DE) fluid will behave as a quintessence field. Then, an effective phantom behavior can only be obtained if  $w_e < -1$ .

## 2.2 The behavior of the coincidence parameter $r$

In order to address the coincidence problem in terms of the dynamics of the parameter  $r \equiv \rho_m/\rho_e$ , we will make in what follows a similar analysis along the line describes in ref. [14]. The dynamics of the parameter  $r$  is given by

$$\dot{r} = r \left( \frac{\dot{\rho}_m}{\rho_m} - \frac{\dot{\rho}_e}{\rho_e} \right), \quad (2.7)$$

where the dot indicates derivative with respect to the cosmic time. Changing the time derivatives by a derivative with respect to  $\ln a^3$ , which will be denoted by a prime, i.e.  $\dot{\rho} = \rho'3H$ , eqs (2.2) and (2.3) go into

$$\frac{\rho'_m}{\rho_m} = -(1 + w_m) + \frac{Q}{3H\rho_m}, \quad \frac{\rho'_e}{\rho_e} = -(1 + w_e) - \frac{Q}{3H\rho_e}. \quad (2.8)$$

In terms of total density  $\rho = \rho_e + \rho_m$ , we obtain

$$\rho' = - \left[ 1 + \frac{w_m r + w_e}{r + 1} \right] \rho. \quad (2.9)$$

For the coincidence parameter  $r$  the evolution equation reads

$$r' = r \left[ (w_e - w_m) + \frac{Q}{3H} \frac{(1+r)^2}{r\rho} \right]. \quad (2.10)$$

Before specifying any particular type of interaction, we will discuss some general properties of these equations. The critical point of Eq. (2.9) is given by

$$r_c = - \frac{(1 + w_e)}{w_m + 1}. \quad (2.11)$$

If  $w_m > 0$  (warm dark matter) and since  $r$  must be positive, it follows that  $w_e < -1$ , which corresponds to a phantom DE. Using the condition  $r' = 0$  in Eq.(2.10) and the value of  $r_c$  one finds

$$\rho_c = - \frac{(w_m - w_e)}{w_m + 1} \frac{Q}{3H(1 + w_e)}. \quad (2.12)$$

Depending on the value of  $w_m \geq 0$  there are two interesting cases.

### 2.3 Case $w_m = 0$

In this case, Eq. (2.12) simplifies to

$$\rho_c = \frac{w_e}{w_e + 1} \frac{Q}{3H}. \quad (2.13)$$

This case was analyzed in [14], concluding that a positive stationary energy density  $\rho_c$  requires  $Q > 0$  since  $w_e < -1$ . This means that independent on the interaction type, the existence of critical points requires a positive exchange from dark energy to dark matter (DM).

### 2.4 Case $w_m > 0$ (warm dark matter)

For this case the expression for  $\rho_c$  becomes

$$\rho_c = \frac{w_e - w_m}{w_m + 1} \frac{Q}{3H(1 + w_e)}. \quad (2.14)$$

The condition  $w_e < -1$  leads in this case to the same result found in section 2.3 for the sign of  $Q$ . This result also holds for  $-1 < w_m < 0$ .

We find here the general condition to have accelerated expansion in terms of the energy densities of the dark components and their EoS. Differentiating (2.1) with respect to  $t$  and substituting for  $\dot{\rho}_m$  and  $\dot{\rho}_e$  gives the auxiliary equation

$$2\dot{H} = -(1 + w_m)\rho_m - (1 + w_e)\rho_e. \quad (2.15)$$

The acceleration is given by the relation  $\ddot{a} = a(\dot{H} + H^2)$ . From (2.1) and (2.15), we obtain

$$\ddot{a} = -\frac{a}{6}(\rho_m(1 + 3w_m) + (1 + 3w_e)\rho_e). \quad (2.16)$$

The condition  $\ddot{a} > 0$  leads to the inequality

$$\rho_e > -\frac{1 + 3w_m}{1 + 3w_e}\rho_m. \quad (2.17)$$

Since we shall consider  $w_e < -1$  this condition represent a right line with positive slope  $1 + 3w_m/3|w_e| - 1$  in the plane  $(\rho_m, \rho_e)$ .

## 3 Evolution equations: Fixed points and stability analysis

Introducing the interaction term  $Q = \lambda\rho_m^\alpha\rho_e^\beta$  in Eqs. (2.2) and (2.3) yields

$$\dot{\rho}_m = -3(1 + w_m)H\rho_m + \lambda\rho_m^\alpha\rho_e^\beta \quad (3.1)$$

$$\dot{\rho}_e = -3(1 + w_e)H\rho_e - \lambda\rho_m^\alpha\rho_e^\beta. \quad (3.2)$$

The time evolution of the dark matter and dark energy densities is given by the highly non-linear coupled differential equations (3.1) and (3.2). We rewrite them as follows:

$$\dot{\rho}_i = f_i(\rho_m, \rho_e), \quad (3.3)$$

where  $i = m, e$ . The functions  $f_m$  and  $f_e$  are defined by the following expressions

$$f_m(\rho_m, \rho_e) = -\sqrt{3}(1 + w_m)\rho_m(\rho_m + \rho_e)^{1/2} + \lambda\rho_m^\alpha\rho_e^\beta \quad (3.4)$$

$$f_e(\rho_m, \rho_e) = -\sqrt{3}(1 + w_e)\rho_e(\rho_m + \rho_e)^{1/2} - \lambda\rho_m^\alpha\rho_e^\beta. \quad (3.5)$$

From numerical results we expect that the above equations have some non-trivial fixed-points  $(\bar{\rho}_m, \bar{\rho}_e)$ , which we want to study analytically including their stability properties. In spite of the non-linearities and according to ref. [23], it is still possible to analyze the stability of fixed points by using the linearized piece of the original differential equations

$$\dot{\rho}_i = \sum_j a_{ij}\rho_j + R_i(\rho_m, \rho_e) \quad (3.6)$$

where  $R_i(\rho_m, \rho_e)$  includes all the non linearities of the original system of equations (3.4) and (3.5), provided the inequality

$$|R_i(\rho_m, \rho_e)| \leq N \left( \sum_i \rho_i^2 \right)^{\frac{1}{2} + \gamma} \quad (3.7)$$

is fulfilled in a neighbour region around the fixed points, for some positive constants  $N$  and  $\gamma$ . To achieve this goal we expand both the dark matter and dark energy densities around their fixed point values  $(\bar{\rho}_m, \bar{\rho}_e)$  as follows:

$$\begin{aligned} \rho_m^\alpha &= (\bar{\rho}_m + \mu\rho_m)^\alpha = \bar{\rho}_m^\alpha + \alpha\mu\rho_m + \mathcal{O}(\mu^2\rho_m^2/\bar{\rho}_m) \\ \rho_e^\beta &= (\bar{\rho}_e + \mu\rho_e)^\beta = \bar{\rho}_e^\beta + \beta\mu\rho_e + \mathcal{O}(\mu^2\rho_e^2/\bar{\rho}_e), \end{aligned}$$

it also holds

$$(\rho_m + \rho_e)^{1/2} = \left( \bar{\rho}_m^\alpha + \bar{\rho}_e^\beta \right)^{1/2} + \frac{1}{2 \left( \bar{\rho}_m^\alpha + \bar{\rho}_e^\beta \right)^{1/2}} \mu (\rho_m + \rho_e) + \mathcal{O}(\mu^2).$$

Inserting the above perturbative expressions into the differential equation system one obtains up to first order in  $\mu$ :

$$\dot{\rho}_i = \sum_j a_{ij}\rho_j \quad (3.8)$$

or explicitly

$$\dot{\rho}_m = -\sqrt{3}(1 + w_m) \left[ \frac{\bar{\rho}_m(\rho_m + \rho_e)}{2(\bar{\rho}_m + \bar{\rho}_e)^{1/2}} + \rho_m(\bar{\rho}_m + \bar{\rho}_e)^{1/2} \right] + \lambda \left[ \beta\rho_e\bar{\rho}_m^\alpha + \alpha\rho_m\bar{\rho}_e^\beta \right] \quad (3.9)$$

$$\dot{\rho}_e = -\sqrt{3}(1 + w_e) \left[ \frac{\bar{\rho}_e(\rho_m + \rho_e)}{2(\bar{\rho}_m + \bar{\rho}_e)^{1/2}} + \rho_e(\bar{\rho}_m + \bar{\rho}_e)^{1/2} \right] - \lambda \left[ \beta\rho_e\bar{\rho}_m^\alpha + \alpha\rho_m\bar{\rho}_e^\beta \right]. \quad (3.10)$$

The tree level values are implicitly defined by the relations

$$\sqrt{3}(1 + w_m)\bar{\rho}_m(\bar{\rho}_m + \bar{\rho}_e)^{1/2} = \lambda\bar{\rho}_m^\alpha\bar{\rho}_e^\beta \quad (3.11)$$

$$\sqrt{3}(1 + w_e)\bar{\rho}_e(\bar{\rho}_m + \bar{\rho}_e)^{1/2} = -\lambda\bar{\rho}_m^\alpha\bar{\rho}_e^\beta, \quad (3.12)$$

or equivalently,

$$\bar{\rho}_e = -\frac{1 + \omega_m}{1 + \omega_e} \quad (3.13)$$

$$\bar{\rho}_m = \left[ (-1)^\beta \frac{\lambda}{\sqrt{3}} \frac{(1 + \omega_m)^{\beta-1} (1 + \omega_e)^{1/2-\beta}}{(\omega_e - \omega_m)^{1/2}} \right]^{(3/2-\alpha-\beta)^{-1}}. \quad (3.14)$$

Now we are prepared to analyze the different numerical results obtained from the direct numerical solution of the system of eqs. (3.3). The numerical solutions were obtained by using a very accurate numerical method of adaptive step-size algorithm called Bulirsch–Stoer method, which will be explained in the next section.

We will use the numerical values  $\omega_m = 0$  and  $\omega_e = -1.1$ , which are of physical interest as we will discuss it in the next section. For these particular values, the above equations have a fixed point given by  $\bar{\rho}_e = 10\bar{\rho}_m$  and

$$\bar{\rho}_m = \left( \lambda \frac{10^\beta}{\sqrt{33}} \right)^{(3/2-\alpha-\beta)^{-1}} \quad (3.15)$$

These fixed points are displayed in figures 3 and 4, and their loci agree remarkably well with the corresponding ones of the numerical results.

In particular, for  $\alpha = 0.9$ ,  $\beta = 1.0$  and  $\lambda = 1$ , eq. (3.15) leads to the relation  $\bar{\rho}_m \approx 0.25$ , which is in agreement with the corresponding locus shown in figure 4. For the next attractor,  $\alpha = 0.8$ ,  $\beta = 1.0$  and  $\lambda = 1$ , eq. (3.15) gives  $\bar{\rho}_m \approx 0.16$ , which again perfectly agree with the numerical result shown in figure 4.

Now we comeback to the linearized system of eqs. (3.9) and (3.10). We rewrite it explicitly as the homogeneous system of differential equations

$$\begin{aligned} \dot{\rho}_m = & \left( -\sqrt{3}(1 + \omega_m) \left[ \frac{\bar{\rho}_m}{2(\bar{\rho}_m + \bar{\rho}_e)^{1/2}} + (\bar{\rho}_m + \bar{\rho}_e)^{1/2} \right] + \lambda\alpha\bar{\rho}_e^\beta \right) \rho_m + \\ & \left( -\sqrt{3}(1 + \omega_m) \left[ \frac{\bar{\rho}_m}{2(\bar{\rho}_m + \bar{\rho}_e)^{1/2}} \right] + \lambda\beta\bar{\rho}_m^\alpha \right) \rho_e \end{aligned} \quad (3.16)$$

$$\begin{aligned} \dot{\rho}_e = & \left( -\sqrt{3}(1 + \omega_e) \left[ \frac{\bar{\rho}_e}{2(\bar{\rho}_m + \bar{\rho}_e)^{1/2}} + (\bar{\rho}_m + \bar{\rho}_e)^{1/2} \right] - \lambda\beta\bar{\rho}_m^\alpha \right) \rho_e + \\ & \left( -\sqrt{3}(1 + \omega_e) \left[ \frac{\bar{\rho}_e}{2(\bar{\rho}_m + \bar{\rho}_e)^{1/2}} \right] - \lambda\alpha\bar{\rho}_e^\beta \right) \rho_m. \end{aligned} \quad (3.17)$$

The stability of the fixed points of the above equations depend on the eigenvalues given by characteristic equation associated to the system:

$$k^2 - (a_{11} + a_{22})k + (a_{11}a_{22} - a_{12}a_{21}) = 0. \quad (3.18)$$

As it is well known, depending on the roots of eq. (3.18), the trajectories around the fixed-point ( $\tilde{\rho}_m = 0$ ,  $\tilde{\rho}_e = 0$ ) will be stable or unstable, (see for instance [23]).

For example, if all roots of the characteristic eq. (3.18) have negative real parts, then the trivial solution  $(\rho_m \ \rho_e)^T = (0 \ 0)^T$  of the linearized system and also of the non-linear system (3.3) is asymptotically stable. On the other side, if at least one of the roots of eq. (3.18) has a positive real part then both systems have an unstable fixed point at  $(0 \ 0)^T$ .



For the interacting model described by eq. (3.3), there are five physical parameters,  $w_m$ ,  $w_e$ ,  $\lambda$ ,  $\alpha$  and  $\beta$ , which should be chosen according to both, physical stability properties on one side, and compatibility with observational data on the other side. The solutions of eq. (3.18) were numerically evaluated for different regions of the parameter space, and found the interesting physical region defined by the inequalities:  $0 \leq \omega_m \leq 1/3$ ,  $-2 - \omega_m < \omega_e < -1$ ,  $\lambda > 1$ ,  $0.0155 < \alpha < 0.222$  and  $0.59 < \alpha < 1.02$  for  $\omega_m = 0$  and  $\beta > 0.8$ . From it, we will consider the subregion  $0 \leq \omega_m \leq 1/3$ ,  $\omega_e = -1.1$ ,  $\lambda = 1$ ,  $\alpha = 0.9$  and  $\beta = 1$ . In particular, in these regions the condition of equation (3.7) holds, which guaranties that the linear analysis of stability also apply to the non-linear differential equation considered.

## 4 Numerical analysis

In this section we present numerical results obtained by using the Bulirsch–Stoer method to solve the non-linear coupled system of eqs. (3.3). The Bulirsch–Stoer method uses an adaptive step-size control parameter, which ensures extremely high accuracy with comparatively little extra computational effort. In the past, this method has proven to be very accurate for solving non-linear differential equations [24]. In addition, we have computed the fixed point trajectories for different values of the five physical parameters  $w_m$ ,  $w_e$ ,  $\lambda$ ,  $\alpha$  and  $\beta$ . The corresponding trajectories within the stability region discussed in the previous section will be shown in the figures below.

The evolution of matter and energy densities  $\rho_m$  and  $\rho_e$  depends critically on the value of the parameter  $w_e$ . In particular, for  $w_e > -1$ , the system exhibits a smooth evolution of the densities towards the fixed point. On the other side, if  $w_e < -1$  the system shows periodic orbits around the fixed point. In this case, a slight variation of the exponents  $\alpha$  and  $\beta$  leads to spiral orbits as it is shown in figures 3 and 4.

### 4.1 Symmetry for $w_e$ and $w_m$

We will now consider the particular values  $\alpha = \beta = 1$ , which has been claimed to give the best fit to observations [10] for an interaction term of the form  $\lambda \rho_m^\alpha \rho_e^\beta$ . As explained above, we have used the Bulirsch–Stoer method to solve numerically 3.3.

For  $\lambda = 1$ ,  $0 < w_m < 1/3$  and  $-1.0 < w_e < -1.1$  the trajectories of the matter and energy densities are displayed in the figures 1 and 2. For the fixed value  $w_m = 0$  and  $w_e$  within the interval  $[-1.1, -1.0]$ , different trajectories are shown in figure 1, which have the remarkable feature of having two intersection points. These points are characterized by the same value of  $\rho_m = 0.4$ . For the fixed value  $w_e = -1.1$  and  $w_m$  within the interval  $[0, 1/3]$ , different trajectories are shown in figure 2. In this case the intersection points arise at the same value of  $\rho_e = 3.5$ .

In both cases the fixed points are of center point type, with the exception of  $w_m = 0$  and  $w_e = -1$ , which correspond to a crossover value (see figure 1).

### 4.2 Spiral trajectories

From the previous subsection, closed trajectories are obtained only for the region defined by  $w_e < -1$ . Depending on the values of  $\alpha$  and  $\beta$ , converging or diverging spirals are obtained. In fact,  $\alpha < 1$  and  $\beta > 1$  lead to convergent spirals and  $\alpha > 1$  and  $\beta < 1$  lead to divergent spirals (see figures 3 and 4).

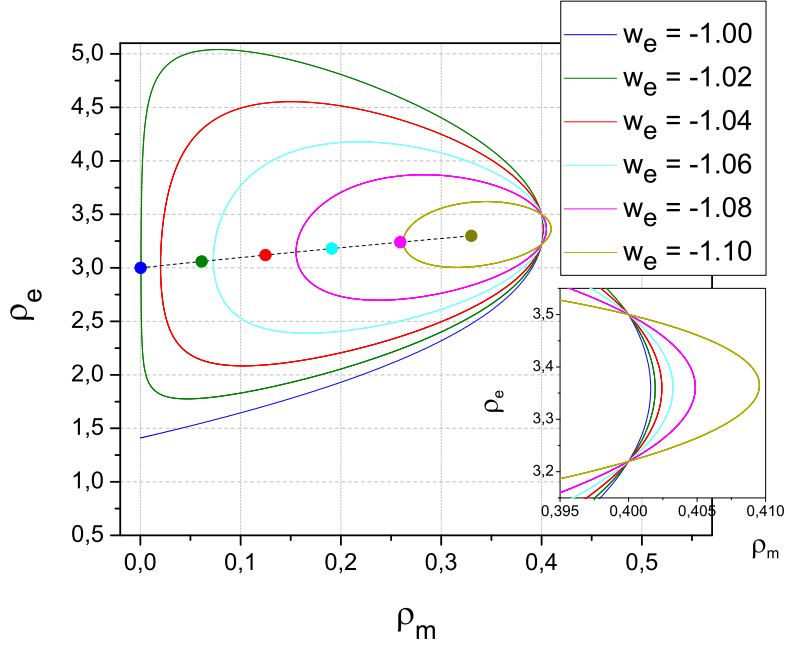


**Figure 1.** (Color on-line) For the parameters  $\alpha = \beta = \lambda = 1$ ,  $w_m = 0$  and  $w_e = [-1.0, -1, 1]$  different evolutions of the densities are shown starting from the same initial values. Two intersection points can be identified for the same value of  $\rho_m$  when the range of  $w_e$  is swept. The dots represent the fixed points given by eq. (3.13) and (3.14).

<b>Stability Region</b>					
$w_m$	$w_e$	$\lambda$	$\alpha$	$\beta$	
[0, 1/3]	[-2- $w_m$ , -1]	$> 1$	[0.0155, 0.222] and [0.59, 1.02]	$> 0.8$	

**Table 1.** Stability region obtain from eq. (3.18).

## 5 Observational Constraints

### 5.1 The Hubble parameter

In a spatially flat FRW Universe, the Hubble constraint and the conservation equations for the matter and dark energy fluids are given by

$$H^2 = \frac{8\pi G}{3}(\rho_m + \rho_e), \quad (5.1)$$

$$\dot{\rho}_m + 3H(\rho_m + p_m) = \lambda\rho_m^\alpha\rho_e^\beta, \quad (5.2)$$

$$\dot{\rho}_e + 3H(\rho_e + p_e) = -\lambda\rho_m^\alpha\rho_e^\beta, \quad (5.3)$$

where  $\lambda$  is a constant to quantify the strength of the interaction between the matter with the dark energy. These equations can be written in terms of the scale factor  $a$  as

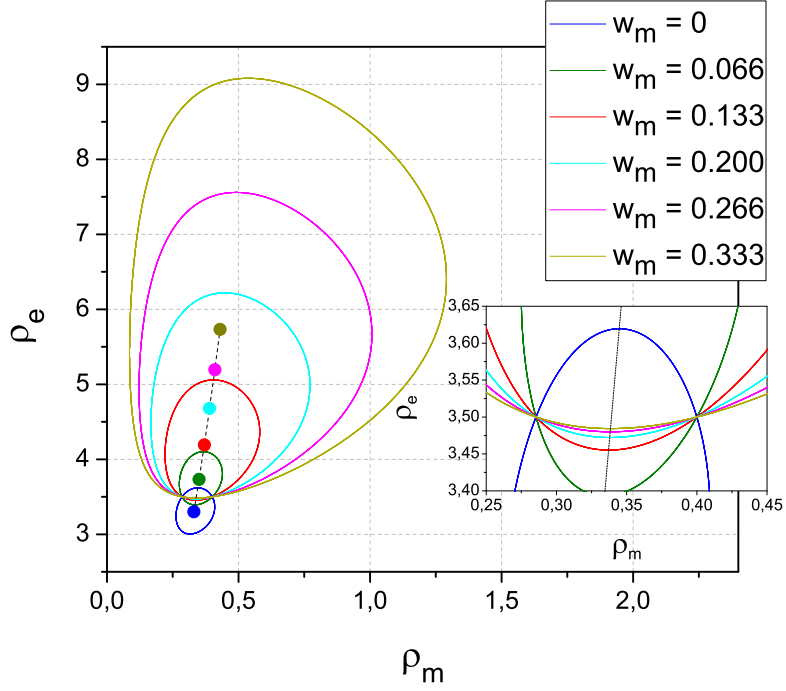


**Figure 2.** (Color on-line) For the parameters  $\alpha = \beta = \lambda = 1$ ,  $w_e = -1.1$  and  $w_m = [0, -1/3]$  different evolutions of the densities are shown starting from the same initial values. Two intersection points can be identified for the same value of  $\rho_e$  when the range of  $w_m$  is swept. The dots represent the fixed points given by eq. (3.13) and (3.14).

$$\frac{d\rho_m}{da} + \frac{3}{a}\rho_m(1 + w_m) = \frac{\lambda \rho_m^\alpha \rho_e^\beta}{aH}, \quad (5.4a)$$

$$\frac{d\rho_e}{da} + \frac{3}{a}\rho_e(1 + w_e) = -\frac{\lambda \rho_m^\alpha \rho_e^\beta}{aH}. \quad (5.4b)$$

where  $\lambda > 0$  as mentioned above. We define the dimensionless parameter  $\bar{\lambda}$  related with  $\lambda$  as

$$\lambda = \frac{\bar{\lambda} H_0}{(\rho_{\text{crit}}^0)^{\alpha-1} (\rho_{\text{crit}}^0)^\beta}, \quad (5.5)$$

where  $\rho_{\text{crit}}^0 \equiv 3H_0^2/(8\pi G)$  is the *critical density* evaluated today and  $H_0$  is the Hubble constant. We define also the dimensionless parameter density  $\hat{\Omega}_i \equiv \rho_i/\rho_{\text{crit}}^0$  with  $i = m, e$ . Using these definitions, the Friedmann constraint equation (5.1) can be expressed as  $H = H_0 \sqrt{\hat{\Omega}_m + \hat{\Omega}_e}$ , and the conservation eqs. (5.4) become

$$\frac{d\hat{\Omega}_m}{da} + \frac{3}{a}\hat{\Omega}_m(1 + w_m) = \bar{\lambda} \frac{\hat{\Omega}_m^\alpha \hat{\Omega}_e^\beta}{a\sqrt{\hat{\Omega}_m + \hat{\Omega}_e}}, \quad (5.6a)$$

$$\frac{d\hat{\Omega}_e}{da} + \frac{3}{a}\hat{\Omega}_e(1 + w_e) = -\bar{\lambda} \frac{\hat{\Omega}_m^\alpha \hat{\Omega}_e^\beta}{a\sqrt{\hat{\Omega}_m + \hat{\Omega}_e}}. \quad (5.6b)$$

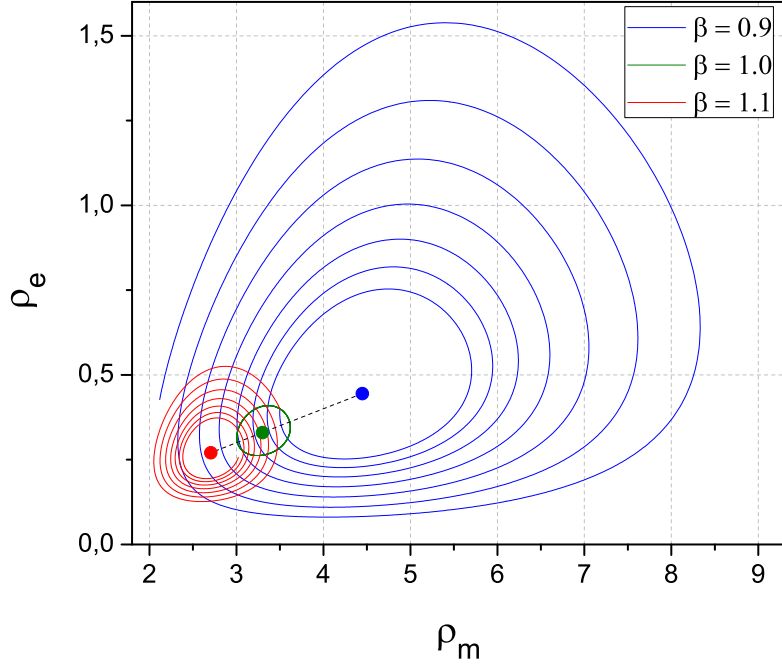


**Figure 3.** (Color on-line) For initial values  $\rho_m = 0.4$  and  $\rho_e = 3.5$  and for the parameters  $\alpha = \beta = \lambda = 1$ ,  $w_m = 0$  and  $w_e = -1.1$ , a closed orbit is shown –blue line– around its fixed point –blue dot–. Starting for the same initial values but changing the value of the power *beta*, spiral trajectories are shown for the evolution of the densities –red and green lines–, for  $\beta = 0.9$  the evolution moves away from the fixed points while for  $\beta = 1.1$  the evolution is towards the fixed point.

Using the relationship between the scale factor and the redshift  $z$  given by  $a = 1/(1+z)$  we express eqs. (5.6) in terms of the redshift as

$$\frac{d\hat{\Omega}_m}{dz} = \frac{1}{1+z} \left[ 3(1+w_m)\hat{\Omega}_m - \bar{\lambda} \frac{\hat{\Omega}_m^\alpha \hat{\Omega}_e^\beta}{\sqrt{\hat{\Omega}_m + \hat{\Omega}_e}} \right], \quad (5.7a)$$

$$\frac{d\hat{\Omega}_e}{dz} = \frac{1}{1+z} \left[ 3(1+w_e)\hat{\Omega}_e + \bar{\lambda} \frac{\hat{\Omega}_e^\alpha \hat{\Omega}_m^\beta}{\sqrt{\hat{\Omega}_m + \hat{\Omega}_e}} \right]. \quad (5.7b)$$

We solve numerically this ordinary differential equation system (ODEs) for the functions  $\hat{\Omega}_m(z)$  and  $\hat{\Omega}_e(z)$ , with the initial conditions  $\hat{\Omega}_m(z=0) \equiv \Omega_{m0} = 0.274$ , and  $\hat{\Omega}_e(z=0) \equiv \Omega_{e0} = 0.726$ .

The dimensionless Hubble parameter  $E \equiv H/H_0$  becomes

$$E(z, w_m, w_e, \bar{\lambda}, \alpha, \beta) = \sqrt{\hat{\Omega}_m(z) + \hat{\Omega}_e(z)}, \quad (5.8)$$

where  $\hat{\Omega}_m(z)$  and  $\hat{\Omega}_e(z)$  are given by the solution of the ODEs (5.7).

## 5.2 Cosmological probes

We constrain the values of the free parameters  $(w_m, w_e, \bar{\lambda}, \alpha, \beta)$  using cosmological observations that measure the expansion history of the Universe, which will be explained in the following sections. We compute their best estimated values through a minimizing process of a

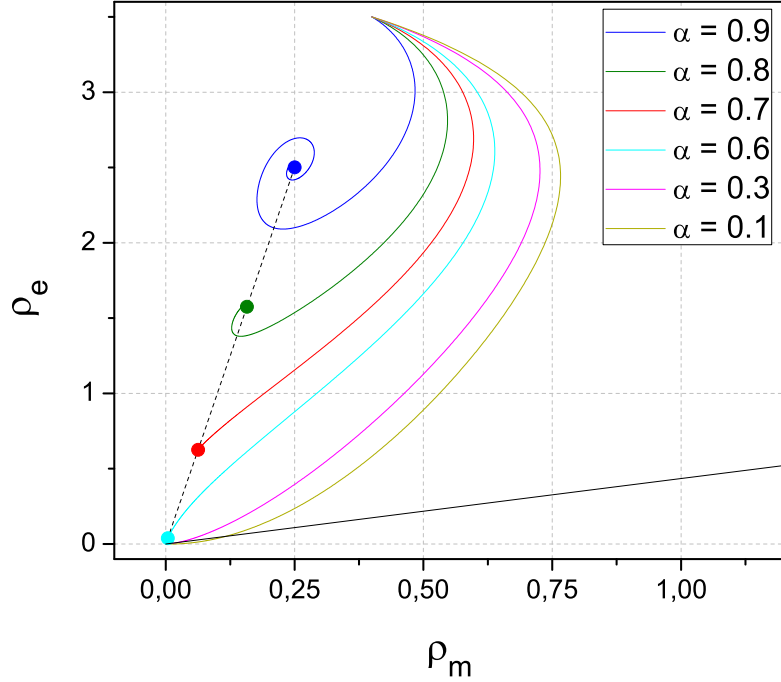


**Figure 4.** (Color on-line) Phase diagrams for  $\rho_m$  and  $\rho_e$  (starting from the same initial conditions) are given by the color lines for different values of  $\alpha$ , and for  $\lambda = \beta = 1$ ,  $w_m = 0$  and  $w_e = -1.1$ . They were obtained by solving numerically eqs. (3.4) and (3.5). For this figure and all the following ones, the black dashed line represents the fixed-point trajectory given in eqs. (3.13) and (3.14). The full black line is the zero-acceleration line given by the expression (2.15) with  $\ddot{a} = 0$ , the region above this line corresponds to an accelerating universe while the region below this line corresponds to a deceleration universe.

$\chi^2$  function defined below, and calculate the marginalized confidence intervals and covariance matrix of the five parameters.

### 5.2.1 Type Ia Supernovae

We use the type Ia supernovae (SNe Ia) of the “Union2.1” data set (2012) from the Supernova Cosmology Project (SCP) composed of 580 SNe Ia [25]. The luminosity distance  $d_L$  in a spatially flat FRW Universe is defined as

$$d_L(z) = \frac{c(1+z)}{H_0} \int_0^z \frac{dz'}{E(z')} \quad (5.9)$$

where  $E(z)$  corresponds to the expression (5.8), and “ $c$ ” to the speed of light in units of km/sec. The theoretical distance moduli  $\mu^t$  for the  $k$ -th supernova at a distance  $z_k$  is given by

$$\mu^t(z) = 5 \log \left[ \frac{d_L(z)}{\text{Mpc}} \right] + 25 \quad (5.10)$$

So, the  $\chi^2$  function for the SNe is defined as

$$\chi_{\text{SNe}}^2(w_m, w_e, \bar{\lambda}, \alpha, \beta) \equiv \sum_{k=1}^n \left( \frac{\mu^t(z_k, w_m, w_e, \bar{\lambda}, \alpha, \beta) - \mu_k}{\sigma_k} \right)^2 \quad (5.11)$$

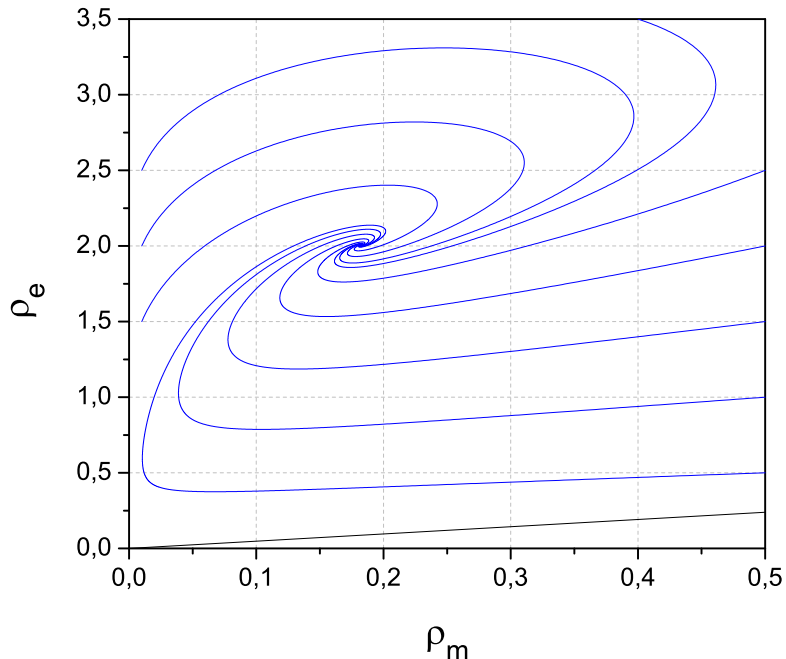


**Figure 5.** (Color on-line) Phase diagrams for the parameters  $\alpha = 0.8$ ,  $\lambda = \beta = 1$ ,  $w_m = 0.1$  and  $w_e = -1.1$ . Spiral evolution of the densities towards the fixed points is shown.

**Best estimates, SNe +  $H(z)$**

$w_m$	$w_e$	$\bar{\lambda}$	$\alpha$	$\beta$	$\chi^2_{\min}$	$\chi^2_{\text{d.o.f.}}$
$0.038^{+10.5}_{-0.038}$	$-1.017^{+1.017}_{-3.94}$	$0.40^{+775.8}_{-0.4}$	$0.28 \pm 1124.06$	$0.73 \pm 10823.3$	573.278	0.97

**Table 2.** The best estimated values for the parameters  $(w_m, w_e, \bar{\lambda}, \alpha, \beta)$ , computed using the joint SNe +  $H(z)$  data sets together. The sixth and seventh columns show the minimum of the  $\chi^2$  function and its corresponding  $\chi^2$  function by degrees of freedom,  $\chi^2_{\text{d.o.f.}}$ , defined as  $\chi^2_{\text{d.o.f.}} \equiv \chi^2_{\min}/(n - p)$  where  $n$  is the number of data ( $n = 592$ ) and  $p$  the number of free parameters estimated ( $p = 5$ ). The errors correspond to 68.3% of confidence level. The covariance matrix is given in expression (5.14) and the figure 7 shows the marginal confidence intervals for pairs of the  $(w_m, w_e, \bar{\lambda}, \alpha, \beta)$  parameters. The nuisance Hubble constant  $H_0$  parameter was marginalized assuming a *flat* prior probability function. From the computed value of  $\chi^2_{\text{d.o.f.}} = 0.97$ , we find that the model has a good fit to data. We also find a very large dispersion on the values of the power parameters  $(\bar{\lambda}, \alpha, \beta)$ , therefore, we are not able to set stronger or useful constraints on these two parameters, both positive and negative values for  $(\alpha, \beta)$  in a large range are almost equally likely. For  $\bar{\lambda}$  we limit ourselves to values of  $\bar{\lambda} > 0$ . For  $w_m$  we find a non vanishing value as best estimate, suggesting a *warm* nature for the dark matter fluid. And for  $w_e$  the best estimated value lies in the phantom regime, however, given the statistical error in its estimation we cannot be conclusive about the phantom nature of the dark energy component. We find interesting that we obtain the stronger constraint (i.e., less dispersion) in its value, compared to the other parameters.

where  $\mu_k$  is the observed distance moduli of the  $k$ -th supernova, with a standard deviation of  $\sigma_k$  in its measurement, and  $n = 580$ .

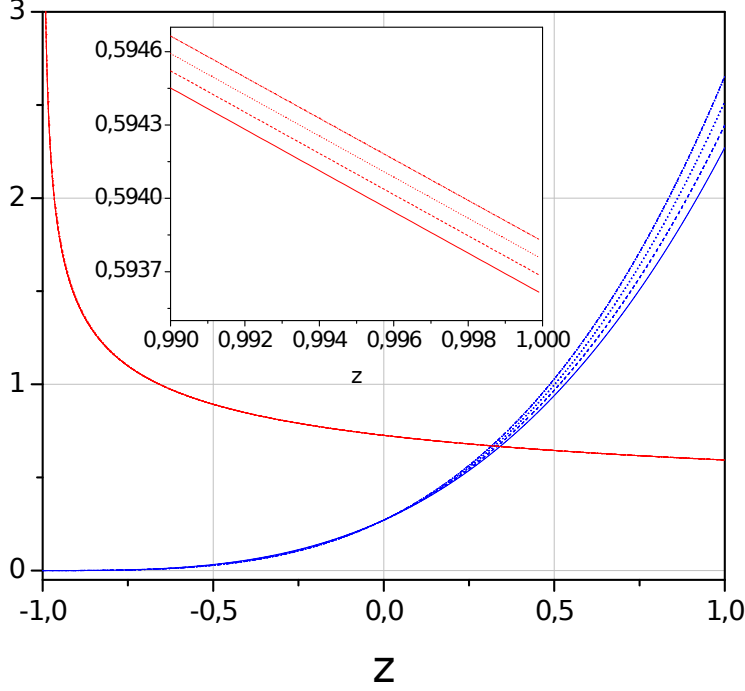


**Figure 6.** (Color on-line) Evolution for  $\hat{\Omega}_m(z)$  (blue) and  $\hat{\Omega}_e(z)$  (red), with the initial conditions  $\hat{\Omega}_m(z=0) \equiv \Omega_{m0} = 0.274$  and  $\hat{\Omega}_e(z=0) \equiv \Omega_{e0} = 0.726$  (present time  $z=0$ ). The parameters are  $\alpha = 0.9$ ,  $\beta = 1$ ,  $w_e = -1.1$  and  $\bar{\lambda} = 1$ . Full lines are for  $w_m = 0.025$ , dashed lines are for  $w_m = 0.050$ , dotted lines are for  $w_m = 0.075$  and dash-dotted lines are for  $w_m = 0.100$ . We find that the dependence of  $\hat{\Omega}_e(z)$  (red) with respect to  $w_m$  remains almost constant compared to  $\hat{\Omega}_m(z)$  (blue) along the interval  $-1 < z < 1$ .

### 5.2.2 Hubble expansion rate

For the Hubble parameter  $H(z)$  measured at different redshifts, we use the 12 data listed in table 2 of Busca et al. (2012) [26], where 11 data come from references [27]–[29]. We assumed  $H_0 = 70 \text{ km s}^{-1} \text{ Mpc}^{-1}$  for the data of Blake et al. (2011) [27] as Busca et al. suggest. The  $\chi^2$  function is defined as

$$\chi_{\text{H}}^2(w_m, w_e, \bar{\lambda}, \alpha, \beta) = \sum_i^{12} \left( \frac{H(z_i, w_m, w_e, \bar{\lambda}, \alpha, \beta) - H_i^{\text{obs}}}{\sigma_{H_i}} \right)^2 \quad (5.12)$$

where  $H_i^{\text{obs}}$  and  $H(z_i, w_m, w_e, \bar{\lambda}, \alpha, \beta) = H_0 \cdot E(z_i, w_m, w_e, \bar{\lambda}, \alpha, \beta)$  are the observed and theoretical values of  $H(z)$  respectively.  $E(z, w_m, w_e, \bar{\lambda}, \alpha, \beta)$  is given by the expression (5.8) and  $\sigma_{H_i}$  is the standard deviation of each  $H_i^{\text{obs}}$  datum.

We construct the *total*  $\chi_{\text{t}}^2$  function that combine the SNe and  $H(z)$  data sets together, as

$$\chi_{\text{t}}^2 = \chi_{\text{SNe}}^2 + \chi_{\text{H}}^2, \quad (5.13)$$

where  $\chi_{\text{SNe}}^2$  and  $\chi_{\text{H}}^2$  are given by expressions (5.11) and (5.12) respectively.

We numerically minimize it to compute the *best estimate values* for the five  $(w_m, w_e, \bar{\lambda}, \alpha, \beta)$  parameters together, and measures the goodness-of-fit of the model to the data. For that, we use a combination of some *built-in* functions of the ©Mathematica software as well as

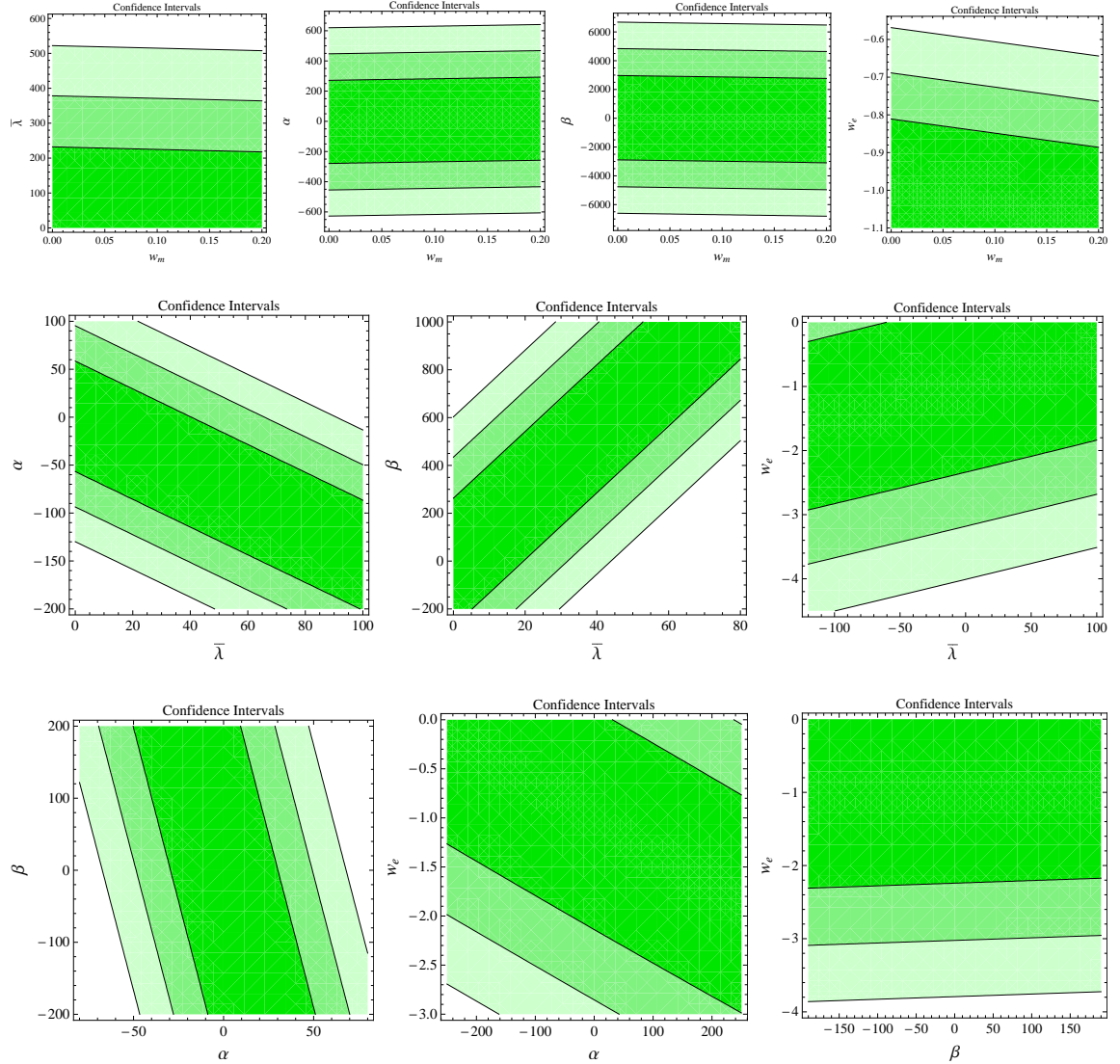


**Figure 7.** (Color on-line). Marginal confidence intervals (CI) from the five parameters space  $(w_m, w_e, \bar{\lambda}, \alpha, \beta)$ , computed together using the joint SNe +  $H(z)$  data sets. In each panel, the contour plots were computed marginalizing over the other two remaining parameters. The CI correspond to 68.3%, 95.4% and 99.7% of confidence level. The best estimated values for  $(w_m, w_e, \bar{\lambda}, \alpha, \beta)$  are shown in table 2 and the covariance matrix  $\mathbf{C}$  is given in (5.14). For the dark matter barotropic index  $w_m$ , we find that non vanishing values are compatible with the observations of SNe +  $H(z)$ . Moreover, marginalizing over the other four parameters we find a value of  $w_m = 0.034^{+0.51}_{-0.034}$  suggesting a preference for a *warm* dark matter instead of a cold one from the present model and data used. On the other hand, we notice a large dispersion in the contour plots, in particular for the power parameters  $(\bar{\lambda}, \alpha, \beta)$ , indicating that a large range of positive and negative values are allowed for both  $(\alpha, \beta)$  with almost the same statistical confidence level; we are not able to set more useful constraints on these three parameters.

the Levenberg-Marquardt Method described in the Numerical Recipes book [30], to minimize the  $\chi^2$  function (5.13).

We use also the definition of “ $\chi^2$  function by *degrees of freedom*”,  $\chi^2_{\text{d.o.f.}}$ , defined as



$\chi_{\text{d.o.f.}}^2 \equiv \chi_{\text{min}}^2/(n - p)$  where  $n$  is the number of *total* combined data used and  $p$  the number of free parameters estimated. For our case ( $n = 592, p = 4$ ).

The numerical results are summarized in table 2 and figure 7. The computed covariance matrix that we found corresponds to

$$\mathbf{C} = \begin{pmatrix} 109.834 & -41.265 & -7975.29 & 11625.6 & -111605 \\ -41.2651 & 15.5193 & 2980.78 & -4349.28 & 41731.6 \\ -7975.29 & 2980.78 & 601931 & -871593 & 8.39609 \times 10^6 \\ 11625.6 & -4349.28 & -871593 & 1.26351 \times 10^6 & -1.21642 \times 10^7 \\ -111605 & 41731.6 & 8.39609 \times 10^6 & -1.21642 \times 10^7 & 1.17145 \times 10^8 \end{pmatrix} \quad (5.14)$$

## 6 Discussion and Conclusions

In order to shed some light on the coincidence problem we have explored a cosmological model composed by a dark matter fluid interacting with a dark energy fluid. Motivated by very recent investigations we have considered a warm dark matter. Since non-linear interactions represent a more physical plausible scenario for interacting fluid we studied an interaction which is given by the term  $\lambda \rho_m^\alpha \rho_e^\beta$ . We have found a general result which indicates the positive critical points of the coincidence parameter  $r = \rho_m/\rho_e$  exist if  $w_e < -1$ , independently of the interaction chosen and the particular EoS used to describe the dark matter. We have considered from the beginning that the energy is transferred from dark energy to dark matter ( $\lambda > 0$ ).

We performed an analytical analysis of the non-linear and coupled differential equations corresponding to the continuity equations for the dark matter and dark energy fluids. In particular we found the fixed points and their stability properties.

Using a high precision numerical method we solved these equations and were able not only to confirm with high accuracy the analytical results but also to extend the solutions beyond the validity regions of the analytical analysis.

The combined method described above allowed us to compute, in the densities space  $(\rho_m, \rho_e)$ , the behaviour of the fixed points in terms of the parameters  $\lambda, \alpha, \beta, w_m$  and  $w_e$ . Closed orbits were found for  $w_e < -1.1$  and  $\alpha = \beta = 1$ . If  $\alpha$  or  $\beta$  are different from the unity, these closed orbits transform into spiral trajectories, evolving towards the origin for  $\alpha < 1$  and  $\beta = 1$ , and away for the fixed point for  $\alpha = 1$  and  $\beta > 1$ . This analysis allowed to constrain the parameters in order to have physically reasonable scenarios, that is accelerated expansion in the late time phase of the cosmic evolution and far future evolution with finite DM and DE densities, which corresponds to spiral trajectories propagating from the fixed points.

The parameters  $(w_m, w_e, \lambda, \alpha, \beta)$  were estimated using the cosmological observations of the Union 2.1 type Ia supernovae and the Hubble expansion rate  $H(z)$  data sets, that measure the late time expansion history of the Universe. A summary of these results are shown on table 2 and figure 7.

For the barotropic index  $w_m$  of the EoS of the dark matter, we found non vanishing and positive values for  $w_m$  that are well compatible with the SNe +  $H(z)$  observations. Marginalizing over the other four parameters, we found that  $w_m = 0.038_{-0.038}^{+10.5}$  which indicates that a *warm* dark matter is well compatible with the observations used here. This is also in agreement with other models and observations indicating a warm nature of the dark matter

fluid. However, we notice a dispersion on the value of  $w_m$  larger than the allowed by other observations.

For the barotropic index  $w_e$  of the dark energy component, we find that the best estimated value of  $-1.017_{-3.94}^{+1.017}$  lies in the phantom regime, however, given the magnitude of the statistical error it is not possible to claim that the phantom nature of the dark energy component is favoured by the observations. We can only claim that the phantom regime is well allowed for the considered values of  $w_e$ .

For the interacting coefficient  $\lambda$ , we defined a dimensionless  $\bar{\lambda}$  for convenience. Using the cosmological observations it is found that the possible values for the interacting coefficient are in the vast range of  $0 < \bar{\lambda} < 800$  with 68.6% of confidence level. This gives us at least an indication of favouring the data the interaction between the dark fluids in this model.

For the power parameters  $(\alpha, \beta)$ , we found a large dispersion in their values that are consistent with the SNe +  $H(z)$  observations with the same confidence level, from positive to negative values of both parameters. So, in the present work we are not able to set strong constraints on  $\alpha$  and  $\beta$  but at least we can assert that a large variety of positive and negative values of the powers  $(\alpha, \beta)$  are allowed according to the data.

From the computed value of  $\chi_{d.o.f.}^2 = 0.97$  ( $\chi_{\min}^2 = 573.278$ ), we find that the model has a well goodness-of-fit to the SNe +  $H(z)$  data.

On the other hand, we use the Bayesian Information Criterion (BIC) [31] to determine which model formed from different cases of the values of  $(w_m, w_e, \bar{\lambda}, \alpha, \beta)$  is favoured by the observations. The value of BIC, for Gaussian errors of the data used, is defined as

$$\text{BIC} = \chi_{\min}^2 + \nu \ln N \quad (6.1)$$

where  $\nu$  and  $N$  are the number of free parameters of the model and the number of data used respectively. The model favoured by the observations compared to the others corresponds to that with the smallest value of BIC, in addition to the criterion that the value of  $\chi_{\min}^2$  should be about or smaller to the number of data used (in our case,  $N = 592$ ) for that model.

Computing the magnitude of the  $\chi^2$  function to measure the goodness-of-fit of data when it is evaluated at some values of interest for  $(w_m, w_e, \bar{\lambda}, \alpha, \beta)$ , as well as the corresponding value of the BIC, we find

- i  $\chi_{\min}^2(w_m = 0.038, w_e = -1.017, \bar{\lambda} = 0.40, \alpha = 0.28, \beta = 0.73) = 573.278$ ; BIC = 605.196: This case corresponds to the present interacting model with five parameters.
- ii  $\chi_{\min}^2(0, -1, 0, 0, 0) = 581.05$ ; BIC = 593.82: This case corresponds to the  $\Lambda$ CDM model; there is not interaction between the dark components.
- iii  $\chi_{\min}^2(0.001, -1.01, 0, 0, 0) = 580.52$ ; BIC = 593.28: This case corresponds to a warm dark matter interacting with a phantom dark energy; there is not interaction between the dark components.
- iv  $\chi_{\min}^2(0.001, -1, 0, 0, 0) = 581.384$ ; BIC = 594.25: A warm dark matter and cosmological constant model, without interaction.
- v  $\chi_{\min}^2(0.038, -1.017, 0.399, 0, 0) = 580.69$ ; BIC = 599.84: A warm dark matter interacting with a phantom dark energy, where the values corresponds to the best estimated in the present work. In this case the interacting term is just the constant  $\bar{\lambda} = 0.399$ , i.e,  $Q = \text{constant}$ .

- vi  $\chi_{\min}^2(0.038, -1, 0.39, 1, 1) = 577.719$ ;  $\text{BIC} = 609.636$ : A warm dark matter interacting with a cosmological constant. The interacting term is of the form  $Q = \lambda\rho_m\rho_e$ . This particular case corresponds to that studied by Lip [13].

Using the BIC as a model selection criterion, we find that the model from the above list with the smallest value of BIC, and therefore most favored by the observations, corresponds to that composed of a *warm* dark matter and a *phantom* dark energy, without interaction. However, the difference with  $\Lambda\text{CDM}$  in the BIC value is too small so that we can just conclude that the warm dark matter – phantom dark energy model described above is as good as  $\Lambda\text{CDM}$  model to fit the SNe+ $H(z)$  data. The interacting model (i) is not as good as the others models, despite it has a good fit to data ( $\chi_{\text{d.o.f.}} = 0.97$ ).

Interestingly, the model that fits worst the data is the case (vi), i.e., the model with an interacting term  $Q = \lambda\rho_m\rho_e$ . This conclusion is in conflict with that of Lip (2011) [13].

In summary, from the dynamical system approach, the non linear interaction chosen in this work leads to plausible scenarios that can alleviate the coincidence problem. The stable fixed points represent universes which end in a dark sector with non zero and finite energy densities in both fluids, despite the phantom behaviour of the dark energy fluid.

On the other hand, using the SNe +  $H(z)$  observations, the best estimated values for the free parameters of the model correspond to a warm dark matter interacting with a phantom dark energy component, with a well goodness-of-fit to data measured through the obtained magnitude of  $\chi_{\text{d.o.f.}}$ . However, using the BIC model criterion we find that this model is overcome by a warm dark matter – phantom dark energy model without interaction, as well as by the  $\Lambda\text{CDM}$  model.

## Acknowledgments

This work was supported by CONICYT through Grant FONDECYT N° 1110840 and by DICYT-USACH grants N° 041231PA and N° 041331CM. A. A. acknowledges the very kind hospitality of Profs. G. P. and N. C. and the Departamento de Física of the Universidad de Santiago de Chile where a substantial part of the work was done. We want finally to acknowledge the referee for valuable comments which contributed to an improvement of our article.

## References

- [1] A. G. Riess et al. [Supernova Search Team Collaboration], *Astron. J.* 116 (1998) 1009; S. Perlmutter et al. [Supernova Cosmology Project Collaboration], *Astrophys. J.* 517 (1999) 565; W. J. Percival *et al.* [The 2dFGRS Collaboration], *Mon. Not. Roy. Astron. Soc.* 327 (2001) 1297; P. Astier *et al.*, [astro-ph/0510447]; A.G.Riess et al. [Supernova Search Team Collaboration], *Astrophys. J.* 607, 665 (2004).
- [2] W. J. Percival *et al.* [The 2dFGRS Collaboration], *Mon. Not. Roy. Astron. Soc.* 327, 1297 (2001); M. Tegmark *et al.* [SDSS Collaboration], *Phys. Rev. D* 69 (2004) 103501; U. Seljak *et al.* [SDSS Collaboration], *Phys. Rev. D* 71 (2005) 103515.
- [3] D. N. Spergel et al., [astro-ph/0603449]; A. C. S. Readhead et al., *Astrophys. J.* 609 (2004) 498; J. H. Goldstein et al., *Astrophys. J.* 599, 773 (2003) ; E. Komatsu *et al.*, [WMAP Collaboration], *Astrophys. J. Suppl.* 189 (2009) 330-376 [astro-ph/0803.0547].
- [4] D.J. Eisenstein *et al.* [SDSS Collaboration], *Astrophys. J.* 633 (2005) 560574, [astro-ph/0501171].

- [5] B. Jain and A. Taylor, Phys. Rev. Lett. 91 (2003)141302, [astro-ph/0306046].
- [6] P.J. Steinhardt, in Critical Problems in Physics, edited by V.L. Fitch and D.R. Marlow (Princeton University, Princeton, NJ, 1997); I. Zlatev, L.-M. Wang, and P. J. Steinhardt, Phys. Rev. Lett. 82, 896 (1999).
- [7] L. Amendola, Phys. Rev. D 62, 043511 (2000); W. Zimdahl, D. Pavón and L.P. Chimento, Phys. Lett. B 521, 133 (2001); M. Gasperini, F. Piazza and G. Veneziano, Phys. Rev. D 65, 023508 (2002); W. Zimdahl, Int. J. Mod. Phys. D 14, 2319 (2005); D. Pavón and W. Zimdahl, Phys. Lett. B 628, 206 (2005); G. Mangano, G. Miele and V. Pettorino, Mod. Phys. Lett. A 18, 831 (2003); G. Farrar and P.J.E. Peebles, Astrophys. J. 604, 1 (2004); S. del Campo, R. Herrera and D. Pavón, Phys. Rev. D 70, 043540 (2004); R. Cai and A. Wang, J. Cosmol. Astropart. Phys. 03, 002 (2005); Micheal S. Berger and H. Shojaei, Phys. Rev. D 73, 083528 (2006); Bo Hu and Y. Ling, Phys. Rev. D 73, 123510 (2006); Hui Li, Z. Guo and Y. Zhang, Int. J. Mod. Phys. D 15, 869 (2006); A. P. Billyard and A. A. Coley, Phys. Rev. D 61, 083503 (2000); M. Szydlowski, Phys. Lett. B 632, 1 (2006); M. Szydlowski, T. Stachowiak and R. Wojtak, Phys. Rev. D 73, 063516 (2006); L. P. Chimento, A. S. Jakubi, D. Pavón and W. Zimdahl, Phys. Rev. D 67, 083513 (2003); L. P. Chimento and D. Pavón, Phys. Rev. D 73, 063511 (2006); G. Olivares, F. Atrio-Barandela and D. Pavón, [gr-qc/0601086]; L. Amendola, G. Camargo Campos and R. Rosenfeld, [gr-qc/061006].
- [8] M. Quartin, M.O. Calvao, S.E. Joras, R.R.R. Reis, I. Waga, *Dark Interactions and Cosmological Fine-Tuning*, JCAP 0805 (2008) 007.
- [9] R. G. Cai and A. Wang, *Cosmology with interaction between phantom dark energy and dark matter and the coincidence problem*, JCAP **0503** (2005) 002 [hep-th/0411025v4]; W. Zimdahl and D. Pavón, *Scaling Cosmology*, Gen. Rel. Grav. **35** (2003) 413-422 [astro-ph/0210484].
- [10] Y. Ma, Y. Gong, and X. Chen, *Couplings between holographic dark energy and dark matter*, Eur. Phys. J. C **69** (2010) 509-519 [astro-ph.CO/0901.1215].
- [11] G. Mangano, G. Miele and V. Pettorino, *Coupled quintessence and the coincidence problem*, Mod. Phys. Lett. A **18** (2003) 831–842 [astro-ph/0212518].
- [12] Laura Lopez-Honorez, Olga Mena, Grigoris Panotopoulos, *Higher-order coupled quintessence*, Phys. Rev. D **82** 123525 (2010) [astro-ph/1009.5263].
- [13] S. Z. W. Lip, *Interacting cosmological fluids and the coincidence problem*, Phys. Rev. D **83**, 023528 (2011), Phys. Rev. D **83**, (2011) 023528 [gr-qc/1009.4942].
- [14] F. Arevalo, A. P. Ramos Bacalhau, W. Zimdahl, *Cosmological dynamics with non-linear interactions*, [astro-ph.COS/1112.5095].
- [15] Xi-ming Chen, Y. Gong and E. N. Saridakis, *Phase-space analysis of interacting phantom cosmology*, JCAP **0904** (2009) 001.
- [16] Z. Guo and Y. Zhang, *Interacting phantom energy*, Phys. Rev. D **71** (2005) 023501.
- [17] U. Alam, V. Sahni, T. Deep Saini, and A. A. Starobinsky, *Exploring the expanding universe and dark energy using the Statefinder diagnostic* Mon. Not. R. Astron. Soc. 354, 063512 (2004).
- [18] P. S. Corasaniti, M. Kunz, D. Parkinson, E. J. Copeland, and B. A. Bassett, Phys. Rev. D 70 , 083006 (2004);
- [19] S. M. Carroll, M. Hoffman, and M. Trodden, Phys. Rev. D 68 , 023509 (2003); P. Singh, M. Sami, and N. Dadhich, Phys. Rev. D 68 , 023522 (2003); J. M. Cline, S. Jeon, and G. D. Moore, Phys. Rev. D 70 , 043543 (2004); M. Sami and A. Toporensky, Mod. Phys. Lett. A 19 , 1509 (2004); S. Das, P. S. Corasaniti, and J. Khoury, Phys. Rev. D 73 , 083509 (2006).
- [20] D. Pavón and B. Wang, *Le Châtelier–Braun principle in cosmological physics*, Gen. Rel. Grav. **41**, (2009) 1–5 [gr-qc/0712.0565].

- [21] P. Colin, V. Avila-Reese, and O. Valenzuela, *Astrophys. J.* 542, 622 (2000), astro-ph/0004115; V. Avila-Reese, P. Colin, O. Valenzuela, E. D’Onghia, and C. Firmani, *Astrophys. J.* 559, 516 (2001), astro-ph/0010525; P. Bode, J. P. Ostriker, and N. Turok, *Astrophys. J.* 556, 93 (2001), astro-ph/0010389; A. Knebe, J. E. G. Devriendt, A. Mahmood, and J. Silk, *Mon. Not. R. Astron. Soc.* 329, 813 (2002), astro-ph/0105316; A. Knebe, J. E. G. Devriendt, B. K. Gibson, and J. Silk, *Mon. Not. R. Astron. Soc.* 345, 1285 (2003), astro-ph/0302443; A. R. Zentner and J. S. Bullock, *Astrophys. J.* 598, 49 (2003), astro-ph/0304292; A. V. Maccio and F. Fontanot, astro-ph/0910.2460; A. L. Serra, M. J. de Leon Dominguez Romero, [gr-qc/1103.5465]; S. Bharadwaj and S. Kar, *Phys. Rev. D* 68, 023516 (2003); K. Y. Su and P. Chen, *Phys. Rev. D* 79, 128301 (2009).
- [22] H. J. de Vega and N.G. Sanchez, *Warm dark matter in the galaxies: theoretical and observational progresses. Highlights and conclusions of the chalonge meudon workshop 2011* [astro-ph/1109.3187].
- [23] L. Elsgoltz, *Ecuaciones diferenciales y cálculo variacional*, Editorial Mir, Moscu. (1969).
- [24] G. Palma and V. H. Cardenas, *Resonance enhancement of particle production during reheating*, *Class. Quantum Grav.* **18** (2001) 2233 [gr-qc/0012005].
- [25] N. Suzuki et al. The Hubble Space Telescope Cluster Supernova Survey: V. Improving the Dark Energy Constraints Above  $z > 1$  and Building an Early-Type-Hosted Supernova Sample. *Astrophys. J.*, 746:85, 2012.
- [26] Busca Nicolas *et al.* 2012, [arXiv:1211.2616]
- [27] Blake C. et al. 2011, *MNRAS*, **418**, 1725
- [28] Blake C. et al. 2012, *MNRAS*, **425**, 405; Chuang, Chia-Hsun, Yun Wang 2012, *MNRAS*, **426**, 226; Reid, B.A., L. Samushia, M. White et al. 2012, [arXiv:1203.6641]; Xu, X., Cuesta, A.J., N. Padmanabhan et al. 2012, [arXiv:1206.6732]
- [29] Adam G. Riess, Lucas Macri, Stefano Casertano, Hubert Lampeitl, Henry C. Ferguson, et al. A 3% Solution: Determination of the Hubble Constant with the Hubble Space Telescope and Wide Field Camera 3. *Astrophys. J.*, 730:119, 2011.
- [30] William H. Press, Saul A. Teukolsky, William T. Vetterling and Brian P. Flannery, *Numerical Recipes 3rd Edition: The Art of Scientific Computing*, 2007, ISBN-10: 0521880688.
- [31] G. Schwarz, *Ann. Stat.*, 6, 461 (1978).